International Core Journal of Engineering
Volume 12 Issue 8, 2026
ISSN: 2414-1895
DOI: 10.6919/ICJE.202608_12(8).0010

Creep Curve Characteristics Analysis of White Sandstone under Coupled Chemical Corrosion and Temperature Effects

Yong Wang*, Qin Xu, Ye Zhou, Chenmeng Zhang, Hui Xi

School of Science, Qingdao University of Technology, Qingdao, 266520, PR China

*Corresponding Author: wang_yong@qut.edu.cn

Abstract

White sandstone in underground structures may be exposed to chemical attack and temperature variation at the same time, but the resulting change in its creep-stage transition has not been clearly quantified. In this work, specimens collected from Zigong, Sichuan Province, were conditioned in H_2SO_4 solution (pH = 1), distilled water, or NaOH solution (pH = 13) at 0 °C, 25 °C, 50 °C, 75 °C, and 100 °C, and were then tested under uniaxial stepwise loading. The complete strain-time records retained the usual sequence of primary, secondary, and tertiary creep in every group. The main difference was the stress at which accelerated deformation began. For specimens treated in distilled water, this threshold was 24 MPa at each temperature. For the acid- and alkali-treated specimens, it remained 24 MPa from 0 °C to 50 °C, decreased to 20 MPa at 75 °C, and reached 16 MPa at 100 °C. Thus, temperature alone did not alter the threshold under neutral conditions within the tested range; its influence became pronounced when a reactive solution was present. The results are consistent with heating-enhanced water-rock reactions that advance internal deterioration and bring forward the transition to unstable creep. These observations provide direct experimental evidence for evaluating chemo-thermal effects on the full creep response of white sandstone.

Keywords

White Sandstone; Creep Curve; Chemical Corrosion; Temperature Coupling; Accelerated Creep.

1. Introduction

Long-term deformation, rather than short-term peak strength alone, often controls the serviceability of rock surrounding underground openings. Under sustained loading, the strain rate generally falls rapidly at first, approaches a nearly constant value, and then rises as failure is approached. The final transition is especially important because it marks the loss of stable deformation. The stress at which this transition begins can therefore be used as an indicator of impending instability. For white sandstone exposed to water or chemically active solutions, that stress may shift as mineral reactions and temperature alter the pore and crack structure. Quantifying this shift is the central issue addressed in the present study.

Previous studies have treated the two environmental factors mainly in isolation. Feng et al. [1-3] documented changes in sandstone mesostructure and macroscopic mechanical response after chemical attack. Creep constitutive descriptions for chemically corroded sandstone were subsequently developed by Wang et al. [4,5], and later models introduced pH-related degradation into the time-dependent response [6,7]. Temperature-related work followed a different route: Qin et al. [8] considered damage evolution under combined temperature and pressure, whereas Zhou et al. [9] proposed a time-dependent model for temperature-stress coupling. Together, these studies show that

ISSN: 2414-1895 DOI: 10.6919/ICJE.202608_12(8).0010

both chemical reactions and heating can affect delayed deformation. They do not, however, define how the onset stress of tertiary creep changes when the two factors act simultaneously below 100 °C, particularly for white sandstone.

Studies outside rock mechanics also provide a useful way to organize a coupled-damage problem, although the materials and governing mechanisms are different. Reviews of additively manufactured metals and alloys [10-14] commonly relate processing history to defects, microstructure, and macroscopic response. Jing et al. [15] discussed the combined contribution of several strengthening mechanisms to creep resistance, while Esmaily et al. [16] summarized reaction-controlled corrosion processes in magnesium alloys. Hao et al. [17] further linked damage mechanics with data-driven fatigue prediction. These publications are not direct evidence for sandstone creep. Their relevance here is limited to the process-structure-property framework and to the treatment of interacting damage mechanisms. That framework is used only as an interpretive reference when relating chemical conditioning and temperature to the measured creep response.

Accordingly, white sandstone from Zigong was examined after conditioning in an acidic solution (H_2SO_4, pH = 1), distilled water, or an alkaline solution (NaOH, pH = 13) at five temperatures between 0 °C and 100 °C. Each specimen was then subjected to uniaxial creep loading through successive stress steps until failure. The analysis focuses on two directly observable features: the form of the complete creep curve and the stress level at which the strain rate begins to accelerate. Comparison of these features across the 15 conditioning groups was used to assess the separate and combined influences of solution chemistry and temperature.

2. Specimen Preparation and Testing Scheme

White sandstone blocks were collected from Zigong, Sichuan Province. Fifteen blocks without visible macroscopic defects and with comparable appearance were chosen for specimen preparation. In accordance with the *Standard for Test Methods of Engineering Rock Mass* (GB/T 50266-2013) [18], cores were cut and ground to cylinders 50 mm in diameter and 100 mm in height. End-face non-parallelism was limited to 0.05 mm, and the axial deviation was kept below 0.25°.

Before chemical treatment, the specimens were dried for 96 hours in an oven maintained at 25 °C. They were then assigned to one of three immersion media: H_2SO_4 solution (pH = 1), distilled water (pH = 7), or NaOH solution (pH = 13). For each medium, specimens were conditioned at 0 °C, 25 °C, 50 °C, 75 °C, and 100 °C. The solution pH was checked daily and adjusted when necessary. Conditioning was terminated after the pH no longer changed in the 100 °C treatment, which was taken as the operational criterion for chemical equilibrium, and the specimens were then removed from the solutions.

Creep loading was carried out on a TAW-200 servo-controlled test system. Preliminary uniaxial compression tests were used to define the loading schedule. The first load was 8 kN, corresponding to approximately 4 MPa for the 50-mm-diameter specimen, and each subsequent step added another 8 kN (4 MPa). The load was applied at 50 N/s and held for 4 hours at each level. Loading continued step by step until the specimen failed. The force-control accuracy of the system was ±50 N, and the test data were recorded automatically throughout the loading history. Table 1 lists the solution and temperature assigned to each specimen group.

ISSN: 2414-1895 DOI: 10.6919/ICJE.202608_12(8).0010

Table 1. Specific settings of temperature and chemical solutions

Specimen group	Immersion solution	pH value	Solution concentration (mol/L)	Solution volume (L)	Temperature (°C)
A0	H2SO4	1	0.1	20	0
A25	H2SO4	1	0.1	20	25
A50	H2SO4	1	0.1	20	50
A75	H2SO4	1	0.1	20	75
A100	H2SO4	1	0.1	20	100
B0	Distilled water	7	0	20	0
B25	Distilled water	7	0	20	25
B50	Distilled water	7	0	20	50
B75	Distilled water	7	0	20	75
B100	Distilled water	7	0	20	100
C0	NaOH	13	0.1	20	0
C25	NaOH	13	0.1	20	25
C50	NaOH	13	0.1	20	50
C75	NaOH	13	0.1	20	75
C100	NaOH	13	0.1	20	100

3. Test Results and Analysis

Because the tests used successive stress levels, the recorded strain histories contained the response to both the current and preceding loads. The Boltzmann superposition principle was therefore applied at each loading stage to separate the creep contribution associated with an individual stress level. The resulting set of stress-specific creep curves is shown in Fig. 1.

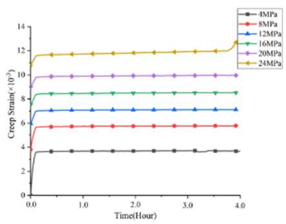

A0

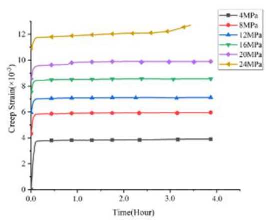

A25

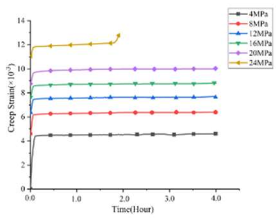

A50

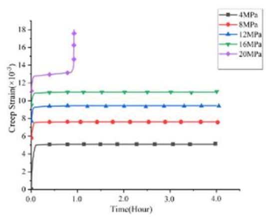

A75

ISSN: 2414-1895 DOI: 10.6919/ICJE.202608_12(8).0010

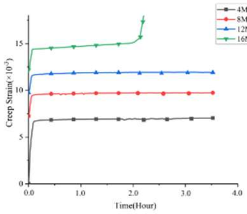

A100

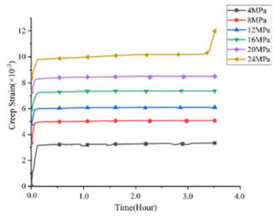

B0

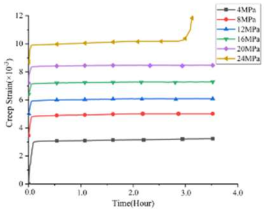

B25

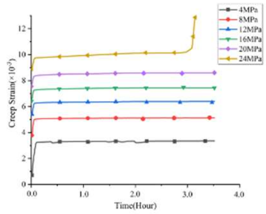

B50

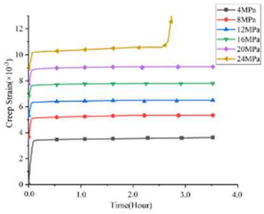

B75

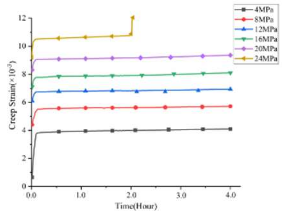

B100

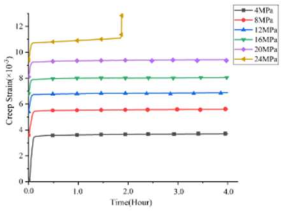

C0

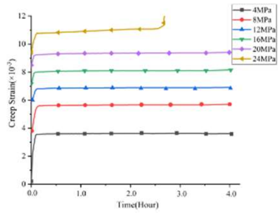

C25

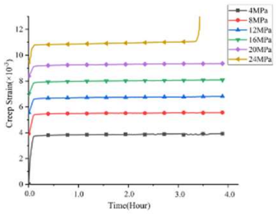

C50

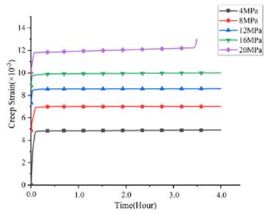

C75

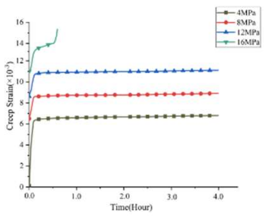

C100

Fig.1 Creep curve of white sand stone

Fig. 1 compares the creep responses of all 15 conditioning groups. The original records extended over several loading stages and contained a large number of measurement points. For plotting, the data were sampled at a fixed interval without changing the loading sequence or the recorded trend. The figure is used to compare curve shape, the instantaneous strain produced by each load increment, and the loading step at which the strain rate turns upward. Differences among the groups are therefore evaluated directly from the measured strain-time histories rather than from a fitted constitutive model.

From the creep curves shown in Fig. 1, the following observations can be made:

(1) Under different coupled chemical corrosion and temperature conditions, white sandstone exhibits three typical creep stages: primary (decelerating) creep, secondary (steady-state) creep, and tertiary (accelerating) creep. At the instant of each load application, instantaneous strain is generated in the specimens under all coupled conditions.

(2) The stress level corresponding to the onset of the tertiary creep stage varies with the coupled conditions. In acidic and alkaline environments, the specimens enter the tertiary creep stage at the sixth loading level (24 MPa) at 0 °C, 25 °C, and 50 °C, and continue until failure. At 75 °C, the tertiary creep stage initiates at the fifth loading level (20 MPa). At 100 °C, the tertiary creep stage begins at the fourth loading level (16 MPa) and proceeds until failure. In neutral environments, the specimens enter the tertiary creep stage at the sixth loading level (24 MPa) at all tested temperatures (0 °C, 25 °C, 50 °C, and 100 °C), and continue until failure.

(3) The underlying mechanisms can be explained as follows. Acidic or alkaline chemical environments induce internal deterioration of the white sandstone, which may lead to either the generation or healing of defects, the formation of new pores, and the enlargement of pre-existing pores. Consequently, the loading level at which the tertiary creep stage initiates differs under various chemical conditions.

4. Conclusion

(1) Under different coupled chemical corrosion and temperature conditions, the uniaxial creep curves of white sandstone consistently exhibit three typical stages: primary (decelerating) creep, secondary (steady-state) creep, and tertiary (accelerating) creep. At the instant of each loading step, an instantaneous strain is generated in the specimen.

(2) The chemical environment significantly affects the stress level at which the tertiary creep stage initiates. Under neutral conditions, specimens at all tested temperatures enter the tertiary creep stage at the sixth loading level (24 MPa). In acidic and alkaline environments, the specimens enter the tertiary creep stage at the same loading level (24 MPa) at 0 °C, 25 °C, and 50 °C; however, the onset stress decreases to the fifth loading level (20 MPa) at 75 °C, and further drops to the fourth loading level (16 MPa) at 100 °C.

(3) Increasing temperature lowers the stress threshold for the onset of tertiary creep in white sandstone. In acidic and alkaline environments, as the temperature rises from 75 °C to 100 °C, the onset stress for tertiary creep declines from 20 MPa to 16 MPa. In neutral environments, in contrast, temperature variation shows no appreciable effect on the onset stress for tertiary creep.

(4) Chemical corrosion and temperature exert a synergistic influence on the creep curve characteristics. Acidic or alkaline environments induce chemical deterioration within the white sandstone, promoting the formation of new pores and the enlargement of existing ones. Temperature below 100 °C accelerates this deterioration process by increasing the rates of chemical reactions, thereby causing the tertiary creep to occur at a lower loading level.

Acknowledgments

Funding: This work was supported by the Qingdao Natural Science Foundation (24-4-4-zrjj-80-jch).

Data Availability Statement

The data used to support the findings of this study are available from the corresponding author upon request.

ISSN: 2414-1895 DOI: 10.6919/ICJE.202608_12(8).0010

Conflicts of Interest

The authors declare that there are no conflicts of interest regarding the publication of this article.

References

[1] Feng, X. T., & Ding, W. X. (2006). Study on mesostructure and macroscopic mechanical properties of sandstone under chemical corrosion. Chinese Journal of Rock Mechanics and Engineering, 25(3), 456–462. (in Chinese)

[2] Ding, W. X., & Feng, X. T. (2009). Damage effect and fracture criterion of fractured rock under chemical corrosion. Chinese Journal of Geotechnical Engineering, 31(6), 899–904. (in Chinese)

[3] Feng, X. T., & Seto, M. (2000). Rock fracture characteristics under chemical environment attack—Part I: Experimental study. Chinese Journal of Rock Mechanics and Engineering, 19(4), 403–407. (in Chinese)

[4] Wang, Y. Y., Lü, Y. M., Xiao, Z. J., et al. (2010). Study on creep model of sandstone under chemical corrosion. Journal of China Coal Society, 35(7), 1095–1098. (in Chinese)

[5] Lü, Y. M. (2010). Study on the influence of chemical corrosion on creep characteristics of deep soft rock [Master's thesis]. Qingdao University of Science and Technology. (in Chinese)

[6] Wang, Y. C., Wang, Y. Y., Li, J. G., et al. (2019). Creep model of shale based on chemical pH characterization. Journal of China Coal Society, 44(S2), 117–124. (in Chinese)

[7] Wang, Y. C., Wang, Y. Y., & Li, J. G. (2019). Study on creep mechanism of shale under chemical corrosion effect. Safety in Coal Mines, 50(8), 67–71. (in Chinese)

[8] Qin, N. (2014). Study on the influence of pressure and temperature on strength, damage energy dissipation and creep of soft rock-like materials [Master's thesis]. Qingdao University of Science and Technology. (in Chinese)

[9] Zhou, G. L., Xu, T., Zhu, W. C., et al. (2017). A time-dependent creep model for rock under temperature–stress coupling. Engineering Mechanics, 34(10), 1–9+25. (in Chinese)

[10] Zhu, T., & Chen, W. (2026). Mechanical behaviour of additively manufactured metals. Nature Materials, 25(3), 373–385.

[11] Mostafaei, A., Ghiaasiaan, R., Ho, I. T., et al. (2023). Additive manufacturing of nickel-based superalloys: A state-of-the-art review on process-structure-defect-property relationship. Progress in Materials Science, 136, 101108.

[12] Xue, X. Y., Bao, J. G., Wu, Z. K., et al. (2026). Additive manufacturing of Ti_2AlNb alloys: A review of process, microstructure, property relationships. Materials Science & Engineering R-Reports, 169, 101197.

[13] Wang, Y. T., Xia, X. Z., Li, R. D., et al. (2025). A review of additive manufacturing heat-resistant aluminum alloys: Materials, properties and strengthening strategies at high temperature. International Materials Reviews, 70(8), 648–709.

[14] George, E. P., Curtin, W. A., & Tasan, C. C. (2020). High entropy alloys: A focused review of mechanical properties and deformation mechanisms. Acta Materialia, 188, 435–474.

[15] Jing, L. J., Cheng, Y. X., Xiao, W. C., et al. (2027). Excellent creep resistance with synergistic strengthening mechanisms of a lightweight single-crystal high-entropy superalloy. Journal of Materials Science & Technology, 279, 220–229.

[16] Esmaily, M., Svensson, J. E., Fajardo, S., et al. (2017). Fundamentals and advances in magnesium alloy corrosion. Progress in Materials Science, 89, 92–193.

[17] Hao, W. Q., Shi, D. Q., Yang, X. G., et al. (2025). Multi-mode fatigue life prediction using machine learning inspired by damage physics. International Journal of Mechanical Sciences, 304, 110723.

[18] Ministry of Housing and Urban-Rural Development of the People's Republic of China, & General Administration of Quality Supervision, Inspection and Quarantine of the People's Republic of China. (2013). Standard for test methods of engineering rock mass: GB/T 50266-2013. China Planning Press. (in Chinese)